Shear-Banded Flow and Transient Rheology of Cationic Wormlike Micellar Solutions

J. I. Escalante,*,† E. R. Macias,† F. Bautista,‡ J. H. Pérez-López,† J. F. A. Soltero,† and J. E. Puig†

Departamentos de Ingeniería Química y de Física, Universidad de Guadalajara, Boul. M. García-Barragán #1451, Guadalajara, Jalisco, 44430 México

O. Manero

Instituto de Investigaciones en Materiales, Universidad Nacional Autónoma de México, Apdo. Postal 70-360, México, D. F. 04510

Received January 11, 2003. In Final Form: May 5, 2003

Linear oscillatory as well as transient and steady shear measurements for micellar solutions of dodecyltrimethylammonium bromide (DTAB) and sodium salicylate (NaSal) as a function of the salt-to-surfactant concentration ratio (C_{SALT}/C_{DTAB}) are presented. Our results indicate that, for molar ratios of salt to surfactant (C_{SALT}/C_{DTAB}) smaller than 1, the micellar solutions follow closely Maxwell behavior with a single relaxation time, that is, they are in the *fast-breaking* regime, and exhibit shear banding above a critical shear rate. When this ratio is greater than 1, micellar solutions behave as semidilute polymer solutions with a spectrum of relaxation times and no stress plateau is observed in steady shear. The results are analyzed with the Granek−Cates model (for linear response) and with a simple model that consists of the upper convected Maxwell constitutive equation coupled to a kinetic equation to account for the breaking and reformation of the micelles (nonlinear behavior). The stress plateau and the critical shear rates are determined from an extended irreversible thermodynamic analysis.

Introduction

Shear-banded flow is one of the most perplexing phenomena observed in many wormlike micellar solutions.[1−6] A key question is the physical origin of the stress plateau associated with shear-banded flows. Cates and co-workers were the first to recognize the physical importance of this stress plateau in wormlike micelles from a theoretical point of view.[7] The stress plateau has also been reported in a variety of surfactant systems such as lamellar phases,[8−11] giant micelles,[12−20] and giant highly deformable vesicles.[21] Moreover, shear-banded flow has been observed in thermotropic liquid crystals[22] and narrow molecular-weight-distribution polymer solutions and melts.[23−25] Hence, this flow mechanism appears to be quite general for complex fluids.

Recent theoretical and experimental results on wormlike micellar solutions have set a controversy about the causes of shear-banded flow.[4,14,15,19,26−31] Several authors have argued in favor of a mechanical instability,[12,13,17,21] whereas others interpret their data as a shear-induced first-order phase transition.[9−11,19,28] This phenomenon was originally explained in terms of a mechanical instability by Cates et al.,[7,32,33] who suggested that, under uniform

* To whom correspondence should be addressed. E-mail: escalant@hotmail.com. Fax: (52)-33-36-50-34-01.

† Departamento de Ingeniería Química, Universidad de Guadalajara.

‡ Departamento de Física, Universidad de Guadalajara.

(1) Richtering, W.; Läuger, J.; Linemann, R. *Langmuir* **1994**, *10*, 4374.
(2) Cates, M. E. *J. Phys.: Condens. Matter* **1996**, *8*, 9167.
(3) Berret, J. F. *Langmuir* **1997**, *13*, 2227.
(4) Olmsted, P. D. *Europhys. Lett.* **1999**, *48* (3), 339.
(5) Ramos, L.; Molino, F.; Porte, G. *Langmuir* **2000**, *16*, 5846.
(6) Rehage, H.; Hoffmann, H. *J. Phys. Chem.* **1988**, *92*, 4712; *Mol. Phys.* **1991**, *74*, 933.
(7) Cates, M. E.; McLeish, T. C. B.; Marrucci, G. *Europhys. Lett.* **1993**, *21*, 451.
(8) Diat, O.; Roux, D.; Nallet, F. *J. Phys. II* **1993**, *3*, 1427.
(9) Roux, D.; Nallet, F.; Diat, O. *Europhys. Lett.* **1993**, *24*, 53.
(10) Sierro, P. Ph.D. Thesis, University of Bordeaux, 1995 (unpublished).
(11) Escalante, J. I.; Hoffmann, H. *Rheol. Acta* **2000**, *39*, 209.
(12) Spenley, N. A.; Cates, M. E.; MacLeish, T. C. B. *Phys. Rev. Lett.* **1993**, *71*, 939.
(13) Hu, Y.; Wang, S.; Jamieson, A. *J. Rheol.* **1993**, *37*, 531.
(14) Berret, J. F.; Roux, D. C.; Porte, G. *J. Phys. II* **1994**, *4*, 1261.
(15) Berret, J. F.; Porte, G.; Decruppe, J. P. *Phys. Rev. E* **1997**, *55*, 1668.
(16) Makhloufi, R.; Decruppe, J.; Aït-Ali, A.; Cressely, R. *Europhys. Lett.* **1995**, *32*, 253.
(17) Liu, C.; Pine, D. J. *Phys. Rev. Lett.* **1996**, *77*, 2121.
(18) Cappelaere, E.; Berret, J. F.; Decruppe, J. P.; Cressely, R.; Lindner, P. *Phys. Rev. E* **1997**, *56*, 1668.
(19) Soltero, J. F. A.; Bautista, F.; Puig, J. E.; Manero, O. *Langmuir* **1999**, *15*, 1604.
(20) Escalante, J. I. M.S. Thesis, University of Guadalajara, 1997 (unpublished).
(21) Bonn, D.; Meunier, J. *Phys. Rev. E* **1998**, *58*, 2115.
(22) Panizza, P.; Archambault, P.; Roux, D. *J. Phys. II* **1995**, *5*, 303.
(23) Tordella, J. P. In *Rheology, Theory and Applications*; Eirich, F. R., Ed.; Academic: New York, 1969. Larson, R. G. *Rheol. Acta* **1992**, *31*, 213.
(24) Larson, R. G. *The Structure and Rheology of Complex Fluids*; Oxford University Press: New York, 1999.
(25) McLeish, T. C. B.; Ball, R. C. *J. Polym. Sci., Polym. Phys. Ed.* **1986**, *24*, 1735.
(26) Bautista, F.; Soltero, J. F. A.; Pérez-López, J. H.; Puig, J. E.; Manero, O. *J. Non-Newtonian Fluid Mech.* **2000**, *94*, 57.
(27) Berret, J. F.; Roux, D. *J. Rheol.* **1995**, *39*, 725.
(28) Macias, E. R. Ph.D. Thesis, University of Guadalajara, 2001 (unpublished).
(29) Cappelaere, E.; Cressely, R.; Makhloufi, R.; Kern, F. *Rheol. Acta* **1994**, *33*, 431.
(30) Schmitt, V.; Schosseler, F.; Lequeux, F. *Europhys. Lett.* **1995**, *30*, 31.
(31) Aït-Ali, A.; Makhloufi, R. *J. Rheol.* **1997**, *41*, 307.
(32) Cates, M. E. *Macromolecules* **1987**, *20*, 2289. Cates, M. E. *J. Phys. (Paris)* **1988**, *49*, 1593. Cates, M. E. *J. Phys. Chem.* **1990**, *94*, 371.
(33) Cates, M. E. In *Theoretical Challenges in the Dynamics of Complex Fluids*; McLeish, T. C. B., Ed.; Kluwer: Dordrecht, The Netherlands, 1997; pp 257−283.

10.1021/la034052o CCC: $25.00
Published on Web 07/11/2003

stress conditions (such as those existing in a cone-and-plate rheometer), the separation of distinct shear bands occurs at shear rates larger than a critical value, $\dot{\gamma}_{c1}$. Moreover, the mechanical instability theory predicts that, when the shear rate reaches a threshold value, $\dot{\gamma}_{c1}$, flow instabilities occur and the stress decreases with increasing shear rate. The stress cannot decrease continuously with increasing shear rate, so eventually there must be an upturn in the curve of σ versus $\dot{\gamma}$. The decreasing section of the stress-versus-shear-rate curve is unstable, and a steady flow can be maintained only if the system splits in bands of low and high shear rates, $\dot{\gamma}_{c1}$ and $\dot{\gamma}_{c2}$, respectively. Others indicate that the shear-banded flow may be akin to a flow-induced first-order phase transition.[27,29,34−36] The coexistence of disordered and oriented phases has been shown with neutron scattering and flow birefringence.[14,29] Moreover, a *master dynamic phase diagram*, where the normalized stress (σ/G_0) levels off progressively up to a plateau that is reduced to a single flat point of coordinates ($\sigma/G_0 = 0.9 \pm 0.05$ and $\dot{\gamma}\tau_R = 3 \pm 0.2$), has been reported, which agrees with the experimental results.[16] In the same context, Fisher and Callaghan have shown by a combination of NMR spectroscopy and NMR velocimetry that the shear-banding phenomena in the cetyltrimethylammonium bromide (CTAB)/D_2O system at concentrations close to the isotropic-to-nematic phase transition are related to a first-order transition, but contrary to previous assumptions based on flow birefringence measurements,[37] the nematic phase does not have a low but rather a high viscosity, probably due to mesoscale ordering.[38,39] An interesting alternative to shear banding is wall slip, in which very thin layers of highly deformed material lubricate the walls of the rheometer.[33]

In this paper, we report the shear rheology of wormlike micellar solutions of dodecyltrimethylammonium bromide (DTAB) and sodium salicylate (NaSal) as a function of the salt-to-surfactant concentration ratio with the goal to switch the system from the *fast*- to the *slow*-breaking regime and to examine the effect on the steady and transient shear flow of these solutions. The linear oscillatory data are analyzed with the Granek−Cates model,[40] whereas the steady and transient simple shears are modeled with the upper convected Maxwell equation coupled to a kinetic equation to account for the breaking and reformation of the micelles.[26]

Modeling

The linear viscoelastic data was fitted with a simplified Poisson renewal model proposed by Granek and Cates, which replaces the exact kinetics of scission and recombination of the micelles by a Poisson jump process that neglects temporal correlations in the chain length experienced by a surfactant monomer or tube segment.[40] The best-fitting of this model to Cole−Cole plots, that is, $G''(\omega)$ versus $G'(\omega)$, yields the parameter ζ ($\equiv\tau_{Break}/\tau_{Rep}$), which allows for the discrimination between kinetic-controlled flow (*fast-breaking regime*) and diffusion-controlled flow (*slow-breaking regime*). From the value of ζ, the breaking time of the micelles was calculated for the various regimes with the following formulas:[41]

$$\zeta \geq 1 \qquad \tau_R \cong \tau_{Rep} \tag{1a}$$

$$\alpha \leq \zeta \leq 1 \qquad \tau_R \cong \tau_{Rep}\zeta^{1/2} \tag{1b}$$

$$\alpha^3 \leq \zeta \leq \alpha \leq 1 \qquad \tau_R \cong \tau_{Rep}\zeta^{3/4}\alpha^{-1/4} \tag{1c}$$

In these equations, $\alpha = l_e/\bar{L}\ (G_{min}''/G_0)/A$, where A is a constant of the order of unity and G_{min}'' is the value of the loss modulus at the dip of the upturn.[41]

The steady and transient nonlinear flow regimes were fitted with a model forwarded by us that consists of the upper convected Maxwell equation coupled to a kinetic equation to account for the breaking and reformation of micelles.[26] For simple shear, the model reads

$$\sigma + \frac{1}{G_0\varphi}\frac{d\sigma}{dt} = \frac{\dot{\gamma}}{\varphi} \tag{2}$$

$$\sigma_{ii} + \frac{1}{G_0\varphi}\frac{d\sigma_{ii}}{dt} = \Theta_{ii} \qquad (i = 1, 2, 3) \tag{3}$$

$$\frac{d\varphi}{dt} = \frac{\varphi_0 - \varphi}{\lambda} + k_0(1 + \mu_1\dot{\gamma}_{12})(\varphi_\infty - \varphi)\sigma_{12}\dot{\gamma}_{12} \tag{4}$$

In these equations, $d\sigma/dt$ is the upper convected derivative of the stress tensor, $\dot{\gamma}$ is the shear rate, φ is the fluidity ($=\eta^{-1}$, η being the shear viscosity), G_0 is the plateau shear modulus, φ_0 and φ_∞ are the fluidities at zero- and infinite-shear rates, respectively, λ is a structure relaxation time, k_0 is the destruction rate constant in the absence of shear-banded flow, and μ_1 is the shear banding intensity parameter. The parameters required to predict experimental data, φ_0, φ_∞, G_0, k_0, and λ, are estimated from rheological experiments.[26,42] The values of φ_0 and φ_∞ were obtained from the steady shear experiments. However, for those samples where the second Newtonian plateau was not reached in the range of shear rates examined, φ_∞ was estimated by the best fitting of the viscous modulus (G'') data with the Hess model.[43] The value of G_0 was obtained from oscillatory shear measurements. The structural relaxation time, λ, was estimated from the intercept of the stress relaxation curve at long times after the cessation of steady shear flow, where the intercept is given by $\exp[-G_0\lambda(\varphi_{ss} - \varphi_0)]$, φ_{ss} being the steady-state fluidity prior to the cessation of shear flow.[42] The parameter k_0, in turn, was evaluated by fitting numerically the stress growth coefficient, η^+, from the inception of the shear flow experiments.[42] The *shear banding intensity* parameter, μ_1, as discussed elsewhere, is uniquely determined by the value of the stress at the plateau region.[44]

For simple steady shear flow, eqs 2 and 4 yield an equation that is cubic in the shear rate:

$$\varphi^2 - \varphi_0\varphi - k_0\lambda(1 + \mu_1\dot{\gamma})(\varphi_\infty - \varphi)\dot{\gamma}^2 = 0 \tag{5}$$

The stress plateau was set by extended irreversible thermodynamic arguments, mainly that the extended Gibbs free energy versus shear rate curve has two minima of equal depth. For simple steady shear flow, this thermodynamic approach gives[44, 45]

(34) Berret, J. F.; Porte, G. *Phys. Rev. E* **1999**, *60*, 4268.
(35) Porte, G.; Berret, J. F.; Harden, J. L. *J. Phys. II* **1997**, *7*, 459.
(36) Olmsted, P. D.; Lu, C.-Y. D. *Phys. Rev. E* **1999**, *60*, 4397.
(37) Decruppe, J. P.; Cressely, R.; Makhloufi, R.; Cappelaere, E. *Colloid Polym. Sci.* **1995**, *273*, 346.
(38) Fisher, E.; Callaghan, P. T. *Europhys. Lett.* **2000**, *50*, 803.
(39) Fisher, E.; Callaghan, P. T. *Phys. Rev. E* **2001**, *64*, 11501.
(40) Granek, R.; Cates, M. E. *J. Chem. Phys.* **1992**, *96*, 4758.
(41) Kern, F.; Lequeux, F.; Zana, R.; Candau, S. J. *Langmuir* **1994**, *10*, 1710.
(42) Bautista, F.; De Santos, J. M.; Puig, J. E.; Manero, O. *J. Non−Newtonian Fluid Mech.* **1999**, *80*, 93
(43) Hess, S. Z. *Physica A* **1977**, 87A, 273.
(44) Bautista, F.; Soltero, J. F. A.; Manero, O.; Puig, J. E. *J. Phys. Chem. B* **2002**, *106*, 13018.
(45) Jou, D.; Casas-Vázquez, J.; Criado-Sancho, M. *Thermodynamics of Fluids Under Flow*; Springer-Verlag: Berlin, 2000.

$$dG = -s\,dT - v\,dP + \frac{v\tau\varphi}{2}(2\sigma_{12}\,d\sigma_{12} + \sum_{i=1}^{3}\sigma_{ii}\,d\sigma_{ii}) \quad (6)$$

Also, at steady state, $\sigma_{11} = 2\dot{\gamma}\sigma_{12}/(G_0\varphi)$ [eq 3 with $i = 1$] and $\sigma_{22} = \sigma_{33} = 0$ [eq 3 with $i = 2, 3$], and because $\sigma_{12} = \dot{\gamma}/\varphi$ from eq 2, then $\sigma_{11} = 2\sigma_{12}^2/G_0$. Hence, the extended Gibbs free energy for simple shear flow (eq 6) under *isobaric* and *isothermal* conditions becomes

$$dG = v\tau\varphi\left(\frac{4\sigma_{12}^3}{G_0^2} + \sigma_{12}\right)d\sigma_{12} \quad (7)$$

In terms of the shear rate, eq 7 can be written, using eq 2, as

$$dG = v\tau\left(\frac{4\sigma_{12}^3}{G_0^2} + \sigma_{12}\right)(1-\beta)\,d\dot{\gamma}_{12} \quad (8)$$

where $\beta = [k_0\lambda(\varphi_\infty - \varphi)(2 + 3\mu_1\dot{\gamma})]/[\varphi^2 + k_0\lambda\dot{\gamma}^2\varphi_\infty(1 + \mu_1\dot{\gamma})]$. It can be easily shown that $\beta \to 0$ as $\dot{\gamma} \to \dot{\gamma}_\infty$ and, because of the range of the parameters of the model given in Table 2, $\beta \ll 1$ as $\dot{\gamma} \to 0$. Hence, eq 8 can be approximated as

$$dG = v\tau\left(\frac{4\sigma_{12}^3}{G_0^2} + \sigma_{12}\right)d\dot{\gamma}_{12} = \frac{v}{G_0\varphi_0}\left(\frac{4\sigma_{12}^3}{G_0^2} + \sigma_{12}\right)d\dot{\gamma}_{12} \quad (9)$$

In eq 9, τ [$\equiv(G_0\varphi_0)^{-1}$] is the Maxwell relaxation time. In a strict sense, τ is a function of the fluidity, φ, and, hence, it is not a constant. However, as a first approximation, only small departures from φ_0 are considered here. Within this approximation, normal stresses can be neglected, and eq 9 reduces to

$$dG = \left(\frac{v}{G_0\varphi_0}\right)\sigma_{12}\,d\dot{\gamma}_{12} \quad (10)$$

Upon substitution of eq 5 into eq 10 and integration of the resulting equation, one gets

$$\Delta G = \frac{v}{G_0\varphi_0}\int\frac{\dot{\gamma}_{12}}{\varphi}\,d\dot{\gamma}_{12} \quad (11)$$

where φ is the solution of eq 5.

Experimental Section

DTAB, 98%+ pure from Tokyo Kasei, was recrystallized from chloroform and ether. NaSal with a purity greater than 99% from Fluka was used as received. Water was bidistilled and deionized. Samples with a surfactant concentration of 12 mM and salt concentrations to give constant values of C_{SALT}/C_{DTAB} (=0.42, 0.85, 1.27, 1.69, and 2.54) were prepared by weighing appropriate amounts of surfactant and NaSal and homogenized by mixing and heating to about 60 °C for 1 h. Then, these solutions were left standing for 1 week at the temperature of the measurements to reach equilibrium.

Steady and transient simple shear as well as small-amplitude oscillatory shear measurements were performed at 30 °C in stress-controlled and in strain-controlled rheometers. Stress-controlled measurements were done in a Rheometrics dynamic stress rheometer RS-5 with two different cone-and-plate devices (40 mm and 0.0384 rad and 25 mm and 0.0997 rad) and in two parallel plates (25 and 40 mm in diameter) with a gap of 0.2 mm in both cases. Strain-controlled measurements were performed in a Rheometrics RDS-II dynamical spectrometer using a cone-and-plate geometry of 0.1 rad and 50 mm in diameter. An environmental control unit was used during the measurements to prevent the evaporation of the solvent. Steady shear rate measurements were made in the range of 0.01−400 s^{-1}. The dynamic data were measured within the linear viscoelastic regime in a frequency range of 0.01−100 rad/s.

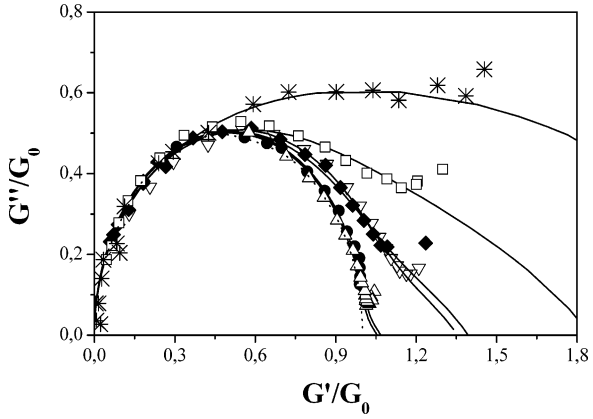

Figure 1. Normalized Cole−Cole plots obtained at 30 °C for 12 mM DTAB micellar solutions with NaSal-to-surfactant molar ratios, C_{SALT}/C_{DTAB}: (●) 0.42; (△) 0.85; (▽) 1.27; (◆) 1.69; (□) 2.54; (∗) 4.2. The solid lines are the best fits to the Granek−Cates model.[40]

Table 1. Parameters Obtained from Oscillatory Experiments and the Best Fit to the Granek−Cates Model[40]

C_{SALT}/C_{DTAB}	η_0 (Pa s)	G_0 (Pa)	τ_R (s)	τ_{relax} (s)	τ_b (s)	ζ
0.42	19.20	0.38	70	72	6.71	0.001
0.85	20.00	0.32	90	82	8.63	0.001
1.27	4.259	0.38	16.8		4.77	0.050
1.69	1.122	0.45	2.9	2.7	1.09	0.092
2.54	0.440	0.96	0.56	0.52	0.47	0.700
4.20	0.163	0.45	0.42		4.20	10.00

Results

Figure 1 depicts normalized Cole−Cole plots (G''/G_0 versus G'/G_0) measured at 30 °C in the linear viscoelastic regime for 12 mM DTAB micellar solutions containing different NaSal concentrations. For C_{SALT}/C_{DTAB} ratios smaller than 1, Cole−Cole data can be fitted accurately by semicircles of radii $G_0/2$, that is,$(G' - G_0/2)^2 + G''^2 = G_0^2/4$, which demonstrates that the solutions follow closely the Maxwell model with a single relaxation time. The fitting of the Granek−Cates model to these curves (lines in Figure 1) yields ζ values smaller than 0.001 (Table 1), indicating that these solutions are in the *fast-breaking* regime. As C_{SALT}/C_{DTAB} is increased above 1, deviations from the Maxwell model are noticeable, which become more severe as this ratio increases. The fit of the Granek−Cates model to the higher C_{SALT}/C_{DTAB} data renders increasingly larger values of the ζ parameter (Table 1), indicating a transition from the *fast-* to the *slow-breaking* regime, where the micellar solutions behave akin to polymer solutions with a spectrum of relaxation times. The values of the main relaxation and breaking times of G_0 and the zero-shear viscosity, η_0, are reported in Table 1. Notice that G_0 does not depend strongly on C_{SALT}/C_{DTAB}, whereas η_0 and τ_R decrease abruptly with increasing salt concentration. Also, notice the large relaxation times (70 and 91 s) of the samples with C_{SALT}/C_{DTAB} ratios of 0.42 and 0.85, respectively.

Steady σ-versus-$\dot{\gamma}$ data measured in simple shear are shown in Figure 2 for 12 mM DTAB solutions with different C_{SALT}/C_{DTAB} ratios. The solid lines in this figure are the predictions of our model with the parameters obtained experimentally, reported in Table 2. At low shear rates,

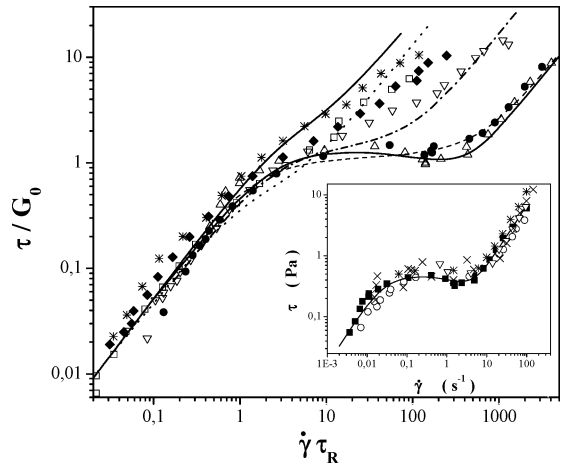

Figure 2. Reduced shear stress versus reduced shear rate measured at 30 °C for 12 mM DTAB micellar solutions as a function of C_{SALT}/C_{DTAB}: (●) 0.42; (△) 0.85; (▽) 1.27; (◆) 1.69; (■) 2.54; (∗) 4.2. The solid lines are the best fits with eq 5. Inset: steady σ-versus-$\dot{\gamma}$ curve for the 12 mM DTAB solution with $C_{SALT}/C_{DTAB} = 0.85$ obtained in the strain-controlled mode with two different cone-and-plate devices [(■) 40 mm and 0.0384 rad and (∗) 25 mm and 0.0997 rad], in two parallel plates [(×) 25 and (▽) 40 mm in diameter] with a gap of 0.2 mm in both cases, and in the stress-controlled mode with a cone-and-plate geometry of (○) 0.1 rad and 50 mm in diameter.

Table 2. Parameters of the Present Model Obtained from Independent Rheological Measurements

C_{SALT}/C_{DTAB}	$\dot{\gamma}_{c1}$ (s^{-1})	$\dot{\gamma}_{c2}$ (s^{-1})	φ_0 ($Pa^{-1}\,s^{-1}$)	φ_∞ ($Pa^{-1}\,s^{-1}$)	$k_0\lambda$ (s Pa^{-1})	μ_1 (s)
0.42	0.04	4.4	0.05	13.5	0.179	0.80
0.85	0.02	4.8	0.06	15.0	0.240	2.00
1.27	0.25	5	0.30	13.0	0.068	0.30
1.69	1	1	0.90	15.5	0.096	0.01
2.54	2.5	2.5	2.98	49.0	0.014	1×10^{-5}
4.20			5.05	76.0	0.005	0

all the solutions are Newtonian; moreover, when the stress divided by the plateau modulus (σ/G_0) is plotted versus the reduced shear rate ($\dot{\gamma}\tau_R$), the data collapse on the same line. At $\dot{\gamma}\tau_R \approx 1$, shear-thinning behavior and a stress plateau develop. However, the transition into the stress plateau is not sharp but rather smooth. The stress plateau occurs at $\sigma/G_0 \approx 1.2 \pm 0.05$, which is slightly larger than the value predicted by the Cates model.[32] Also, the reduced shear rate interval for the stress plateau is larger and better defined at low C_{SALT}/C_{DTAB} ratios. At high shear rates, above a second critical value, an upturn in the shear stress follows, where Newtonian behavior is observed again. However, as the ratio of salt to surfactant concentrations is increased, the stress plateau tends to vanish and, at a C_{SALT}/C_{DTAB} ratio larger than about 1.2, an inflection in the σ-versus-$\dot{\gamma}$ relationship, rather than a plateau, is observed. Notice that the theoretical stress plateau, fixed by the criterion of an equal extended Gibbs free energy minimum between the bands, passes through the experimental data.

To show that the stress plateau could be related to a mechanical instability, the steady σ-versus-$\dot{\gamma}$ curve for the 12 mM DTAB solution with $C_{SALT}/C_{DTAB} = 0.85$ was obtained in a shear rate-controlled instrument and in stress-controlled rheometer using two different geometries (inset in Figure 2). In both the low- and high-shear-rate Newtonian regions, the data obtained with both instruments coincide. However, in the shear-banding region, only data obtained with a shear-rate-controlled mode can span the whole shear-rate range of the stress plateau. By contrast, when obtaining data with the stress-controlled instrument was tried, there were random jumps in the response of the instrument; that is, the response jumped back and forth between the low- and the high-shear-rate branches. As a result, only a few data points were obtained in the shear-banding region with the stress-controlled instrument. On the other hand, the extended irreversible thermodynamic analysis outlined before and described elsewhere[44] indicates that two extended free energy minima of different depths coexist in the metastable region. The metastable states can be explained considering that the flow causes fluctuations in all the variables, especially concentration fluctuations. The most probable fluctuations are small and decrease exponentially with the height of the free energy barrier,[46] and then the system can remain for some time with the original structure. When large fluctuations occur, an incipient induced structure forms that acts as a nucleus for the growth of the high-shear-rate band. These metastable states are kinetically favored, whereas at the stress plateau, the coexistence of the states is thermodynamically preferred.

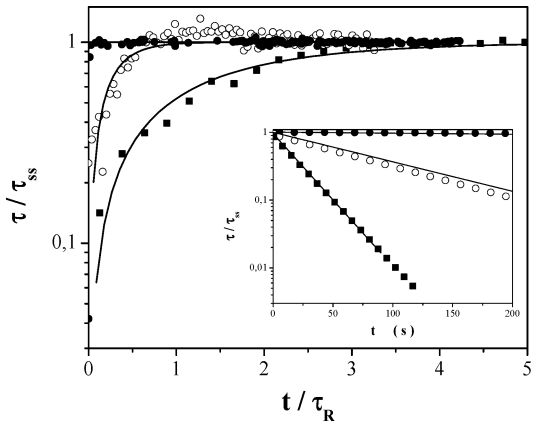

Figure 3. Normalized stress growth after the inception of shear flow for 12 mM solutions containing different C_{SALT}/C_{DTAB} ratios: (●) 0.42; (○) 0.85; (■) 1.69. The applied shear rate (0.005 s^{-1}) is in the low-shear-rate Newtonian region. Inset: normalized stress relaxation after the cessation of steady shear flow. The solid lines in the figure and inset are the fits of the Maxwell model using the main relaxation time of the samples obtained from oscillatory measurements.

Figures 3 and 4 show stress growth after the inception of shear flow for 12 mM DTAB solutions containing different C_{SALT}/C_{DTAB} ratios for shear rates within the low-shear Newtonian region and for shear rates within the shear-banding region, respectively. When the applied shear rate is in the low-shear Newtonian region, the steady-state stress is reached very rapidly, that is, within one or two relaxation times, and no overshoots are observed (Figure 3). The stress relaxation after the cessation of steady shear flow is single-exponential (inset in Figure 3) with relaxation times that are comparable to those obtained by oscillatory shear (Table 1). However, when the applied shear rate is within the shear-banding region, stress overshoots and oscillations are detected and 10 or more relaxation times are required to achieve steady state (Figure 4A). Figure 4B shows an amplification of the scale for the sample containing $C_{SALT}/C_{DTAB} = 2.54$, where only one overshoot and no oscillations are observed because there is no shear-banding region for this sample (Figure 2). Moreover, the stress relaxation after the cessation of steady shear is no longer single-exponential, except for the solution with $C_{SALT}/C_{DTAB} = 2.54$ (Figure 4C), which has no shear-banding region (Figure 2).

(46) McQuarry, D. A. *Statistical Thermodynamics*; University Science Books: Mill Valley, CA, 1976.

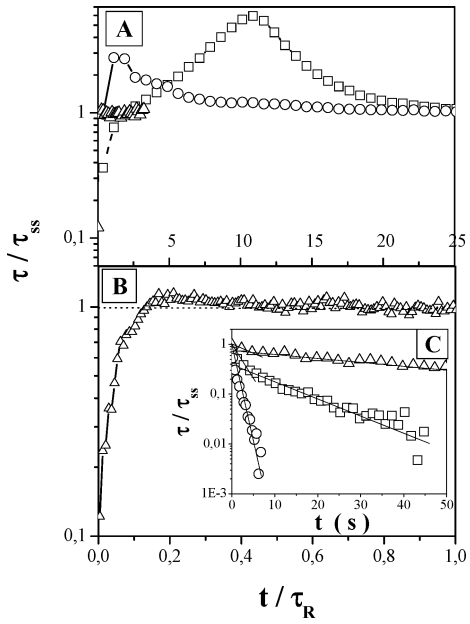

Figure 4. (A) Normalized stress growth after the inception of shear flow for 12 mM solutions containing different C_{SALT}/C_{DTAB} ratios: (△) 0.85; (□) 1.69; (○) 2.54. The applied shear rate is within the shear-banding region. (B) Amplification of data for $C_{SALT}/C_{DTAB} = 0.85$. (C) Normalized stress relaxation after the cessation of steady shear flow. The solid lines in the inset are the fits of the model forwarded here.

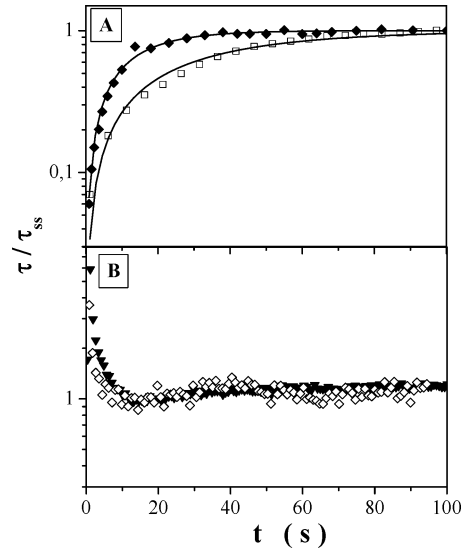

Figure 5. Stress growth for 12 mM solutions with $C_{SALT}/C_{DTAB} = 0.85$ as a function of the applied shear rates in inverse seconds: (A) (□) 0.005; (◆) 0.01. (B) (▼) 20; (◇) 100.

Figures 5 and 6 display the stress growth as a function of the applied shear rate for a 12 mM CTAB solution with $C_{SALT}/C_{DTAB} = 0.85$. For shear rates within the first Newtonian region ($\dot{\gamma}$ of 0.005 and 0.01 s^{-1}), the stress growth follows the Maxwell model (solid lines in Figure 5A) using the main relaxation time obtained from oscillatory measurements (Table 1), and steady state is reached very rapidly (Figure 5A). Figure 5 also depicts the stress growth for shear rates within the high-shear-rate Newtonian region ($\dot{\gamma}$ of 20 and 100 s^{-1}); in this case, steady state is reached within a fraction of the relaxation time of the sample but overshoots, and small oscillations are detected (Figure 5B). By contrast, when the applied shear rate is within the shear-banding region ($\dot{\gamma} = 0.1, 1, 5\ s^{-1}$), overshoots, oscillations, and long transients appear

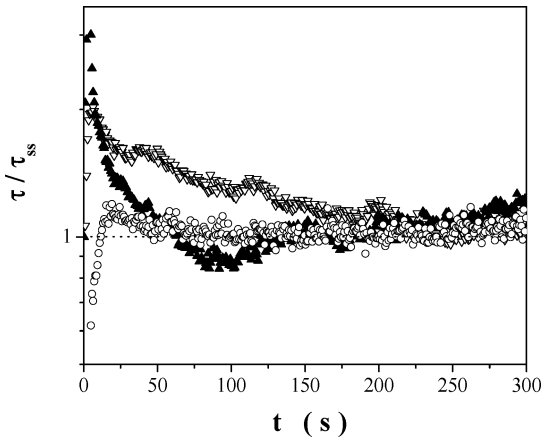

Figure 6. Stress growth for 12 mM solutions with $C_{SALT}/C_{DTAB} = 0.85$ as a function of the applied shear rate in inverse seconds: (○) 0.1; (▽) 1; (▲) 5.

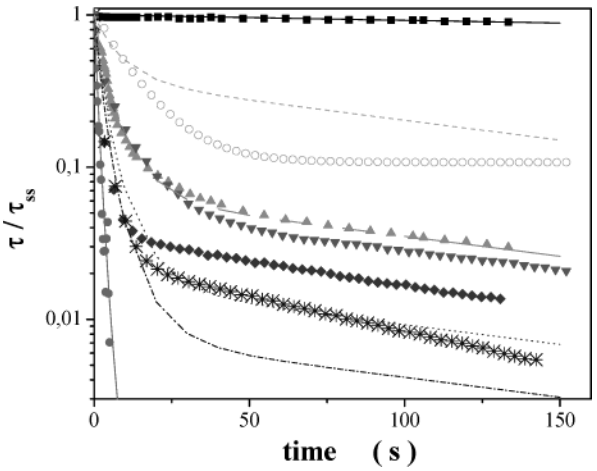

Figure 7. Stress relaxation after the cessation of steady shear flow for 12 mM solutions with $C_{SALT}/C_{DTAB} = 0.85$ as a function of the applied shear rate in inverse seconds: (■) 0.005; (○) 0.01; (▲) 0.1; (▼) 2; (◆) 5; (∗) 20; (●) 100. The solid lines are the predictions of eq 12.

(Figure 6). The transients and oscillations last for more than 1000 s (not shown).

Figure 7 depicts stress relaxation measurements after the cessation of steady shear flow for a 12 mM DTAB micellar solution with $C_{SALT}/C_{DTAB} = 0.85$. When the shear rate is within the low-shear Newtonian region, $\dot{\gamma} = 0.005\ s^{-1}$, stress relaxation is single-exponential, and the stress relaxation curve can be reproduced with the Maxwell model using the relaxation time obtained from oscillatory measurements (Table 1). At high shear rates, above the multivalued region, $\dot{\gamma} = 100\ s^{-1}$, and the relaxation is fast and single-exponential also. However, when the applied shear rate is within the multivalued region, $\dot{\gamma} = 0.01$ to about 10 s^{-1}, the stress exhibits two main relaxation mechanisms, one fast and another slow. Notice that the slopes of the fast and slow relaxation mechanisms in the multivalued region are similar (but not identical) to those of the very high- and very low-shear-rate Newtonian regions, respectively, which suggests that two structures, which do not change much as the shear rate is increased, coexist within the shear-banding region. To substantiate this hypothesis, we predicted the stress relaxation curves with our model, with the assumptions that two different phases coexist (the low- and the high-shear-rate fluids) and that the lever rule proposed by Porte et al. is valid.[35] With these assumptions, the solution of our model for

stress relaxation after the cessation of steady shear flow yields

$$\tau/\tau_{ss} = \exp -\{\varphi_0 t + [x\varphi_0 + (1 - x)\varphi_\infty - \varphi_0]\lambda e^{-t/\lambda}\}G_0 \quad (12)$$

Here, τ_{ss} and $\dot{\gamma}_{ss}$ are the steady shear stress and shear rate before the cessation of flow and the fraction of fluid supporting the lower critical shear rate, x, is given by the lever rule as

$$x = \frac{\dot{\gamma}_{ss} - \dot{\gamma}_{c2}}{\dot{\gamma}_{c1} - \dot{\gamma}_{c2}} \quad (13)$$

Predictions are excellent for shear rates within the low- and high-shear-rate Newtonian regimes (Figure 7), where $x = 1$ and 0, respectively, in eq 12. In the shear-banding region, and in the proximities of the stress plateau, the model predicts two main relaxation times. Predictions are quite good at shear rates where the values of the plateau stress and the metastable stress are similar; however, as the stress plateau and the metastable (*top jumping*) stress become further apart, the predictions deviate from the experimental data (Figure 7). Notice, however, that the stress relaxation curve of the sample subjected to shear rates of 0.01 and 20 s^{-1}, which presumably are outside the multivalued region, also depicts two relaxation mechanisms (open circles and asterisks in Figure 7, respectively). This can be due to an underprediction of the magnitude of the multivalued region by our model. That our model also predicts two relaxation mechanisms for these samples (dashed lines in Figure 7) is due to a small viscoelastic contribution inherent in our model that is present even in the low- and high-shear-rate Newtonian branches.

Discussion and Conclusions

Shear-banded flow is a fascinating but still not completely understood phenomenon. Shear-banded flow (or spurt effect) was first observed in monodisperse linear polymer melts ($M_w/M_n < 1.15$).[47−50] For these systems, McLeish and Ball predicted a discontinuity in the flow curve obtained by capillary rheometry with the Doi−Edwards theory extended to include relaxation processes associated with chain length equilibration.[25] These authors found that the discontinuity is very sensitive to the ratio of the reptation time (τ_{Rep}) to the equilibration time (τ_{eq}). However, these two characteristic times depend strongly on molecular weight ($\tau_{Rep} \sim M^3$ and $\tau_{eq} \sim M^2$) and so, molecular weight polydispersity, which is common in high-molecular-weight polymers, can mask the discontinuity in the $\sigma-\dot{\gamma}$ relationship.

In the absence of salt, DTAB forms spherical micelles in water at the concentrations studied here. The effect of adding salt is to screen the interactions between the headgroups of the micelles, thus allowing the micelles to grow.[51] Moreover, salts also screen the interactions among the micelles, thus facilitating the orientation of the micelles under shear, and phase transitions to ordered phases can be induced at lower surfactant concentrations. In fact, Decruppe et al. showed by optical and rheological measurements that the shear-induced nematic phase forms at lower surfactant concentrations in the CTAB system upon the addition of potassium bromide.[52] Also, they reported a sharp break when the shear rate reaches $\dot{\gamma}_{c1}$ in the CTAB/water system and small curvatures in the CTAB/water system containing an equimolar amount of KBr. These authors concluded that the curvature indicates that the shear stress increases more slowly than the shear rate because the average orientation of the long wormlike micelles becomes more and more important before reaching the transition.

Here, we showed that by varying the salt-to-surfactant molar ratio (C_{SALT}/C_{DTAB}), the micellar solution can shift from the *fast-breaking* regime, where the system behaves as a Maxwell fluid with a single relaxation time given by $\tau_R = (\tau_{Rep}\tau_{Break})^{1/2}$, to a *slow-breaking* regime, where the system behaves as a polydisperse polymeric solution with a spectrum of relaxation times (Figure 1). Evidently, at the lowest C_{SALT}/C_{DTAB} (=0.42) ratio used here, the micelles are fully entangled.[53] For $C_{SALT}/C_{DTAB} > 1$, deviations from Maxwell behavior become more severe as this ratio augments. The fitting of Cole−Cole plots with the Granek−Cates model indicates that the ζ parameter increases rapidly with salt concentration for $C_{SALT}/C_{DTAB} > 1$ (Table 1), demonstrating the shifting from the *fast-* to the *slow-breaking* regimes.

Similar to high-molecular-weight polymer systems, wormlike micellar solutions also exhibit a broad size distribution, but because of the chain-breaking and recombination processes that average the chain length distribution, these systems exhibit a narrow distribution of characteristic times in the *fast-breaking* regime; that is, they behave as highly monodisperse systems.[32] Hence, wormlike micellar solutions are excellent candidates for examining the spurt effect. Figure 2 reveals that, when the micellar solution dynamics is kinetically controlled, only one relaxation time dominates and shear-banding flow develops at one critical shear rate and disappears at another critical shear rate. Above this second critical rate, the high-shear-rate Newtonian branch forms. As the salt-to-surfactant ratio is raised, the ζ parameter increases, the shear-banding region becomes smaller, and the transition is less sharp. When $C_{SALT}/C_{DTAB} > 1$, the ζ parameter tends to 1, indicating that the solution is in the *slow-breaking* regime; that is, the dynamics are diffusion-controlled. In this case, no shear-banded flow is observed at all and only an inflection at the low critical shear rate is detected (Figure 2). When the reduced variables (σ/G_0 and $\dot{\gamma}\tau_R$) suggested by Berret et al. are used,[15] a master curve is obtained; however, the values of the reduced critical shear stress ($\sigma_c/G_0 = 1.2 \pm 0.05$) and of the reduced first critical shear rate ($\dot{\gamma}_{c1}\tau = 3$) are larger than those predicted by the Cates model and also larger than the values for the master curve proposed by Berret and collaborators. Notice also that the second critical shear rate ($\dot{\gamma}_{c2}\tau$) also appears at the same value for the two samples that shear-banded (Figure 2).

A controversial issue in shear-banded flow is how to determine from first principles the shear stress plateau and the low- and high-shear-rate branches. Recently, using extended irreversible thermodynamics equations develop for shear flow of polymer solutions[45] in conjunction with our model, we were able to predict quite accurately the experimental stress plateau in cetyltrimethylammonium tosilate micellar solutions.[44] Here, with the same approach, we predict correctly the stress plateau in DTAB/NaSal

(47) Bagley, E. B.; Cabot, I. M.; West, D. C. *J. Appl. Phys.* **1958**, *29*, 109.
(48) Tordella, J. P. In *Rheology Theory and Applications*; Eirich, F., Ed.; Academic: New York, 1969; Vol. 5, p 57.
(49) Vinagrov, G. V. *J. Polym. Sci.* **1972**, *10*, 1061.
(50) Vinagrov, G. V. *Rheol. Acta* **1973**, *12*, 273.
(51) Israelachvili, J. N. *Intermolecular and Surface Forces*; Academic Press: New York, 1992.
(52) Decruppe, J. P.; Capelare, E.; Cressely, R. *J. Phys. II* **1997**, *7*, 257.
(53) Shikata, T.; Hirata, H.; Kotaka, T. *Langmuir* **1987**, *3*, 1081.

micellar solutions (Figure 2). It is noteworthy that extended irreversible thermodynamics predicts a criterion of equal areas above and below the stress plateau, similar to the Hemholtz equal-areas criterion in *P*-versus-ρ plots in first-order phase transitions,[54] only when normal stresses can be neglected. Details are given elsewhere.[44]

Shear-banded flow is usually accompanied by oscillations and long transients.[16,19,31,34,52,55−59] Porte and Berret have analyzed these phenomena and concluded that they resemble the kinetics of nucleation and growth of a second phase, similar to phenomena occurring in equilibrium first-order phase transitions.[34] Here, we showed that when the solutions (regardless of the C_{SALT}/C_{DTAB} ratio) are in the low-shear-rate Newtonian branch, the stress growth after the inception of shear flow is fast and follows Maxwell behavior with a single relaxation time (Figure 3). Moreover, after the cessation of shear flow, the solutions relax monoexponentially, and it can be reproduced with the Maxwell model and the crossover relaxation time obtained from linear oscillatory measurements (inset in Figure 3). However, once the applied shear rate is above the critical value for shear banding ($\dot{\gamma}_{c1}\tau_R > 3$), oscillations and overshoots are observed (Figure 4A). Moreover, transients last more than 20−40 relaxation times before steady state is reached. Nevertheless, samples that do not exhibit shear banding relax nearly single-exponentially after the cessation of shear flow (see data for $C_{SALT}/C_{DTAB} = 2.54$ in Figure 4C), indicating a very different relaxation mechanism than that in those samples that shear-banded.

Stress growth as a function of the applied shear rate for the 12 mM DTAB solution with $C_{SALT}/C_{DTAB} = 0.85$ also exhibits a fast response and near Maxwell behavior when the applied shear rate is below $\dot{\gamma}_{c1}$ (Figure 5A) or above $\dot{\gamma}_{c2}$, although a single overshoot is detected in the latter (Figure 5B). However, when the applied rate is within the shear-banding region, overshoots and undershoots, oscillations, and long transients are observed (Figure 6). Grand et al. proposed that the presence of overshoots and oscillations is related to the proximity (in shear stress) of the metastable branch.[57] The extended Gibbs free energy has two minima of different depths at this shear rate; the less deep minimum (less stable) occurs at the high-shear-rate branch.[44] Under these circumstances, it is expected that, when a shear rate is applied, the system tends to the dynamical equilibrium at such a shear rate. This corresponds to the local minimum at the metastable branch. However, the overall extended Gibbs free energy minimum is located at the critical shear rates, $\dot{\gamma}_{c1}$ and $\dot{\gamma}_{c2}$, and so, the system tends to move to the overall minimum. The nucleation and growth of the shear-aligned phase is the path to achieve this overall minimum, which is reflected in oscillations around the minimum and long transients.

The stress relaxation curve after the cessation of steady shear flow is single-exponential when the applied shear rate is smaller than $\dot{\gamma}_{c1}$ or larger than $\dot{\gamma}_{c2}$ (Figure 7). When the applied shear rate is within these two critical values, two relaxation mechanisms are detected (Figure 7). The similarities of the relaxation slope when $\dot{\gamma}_{applied} < \dot{\gamma}_{c1}$ with the slow mechanism and the relaxation slope when $\dot{\gamma}_{applied} > \dot{\gamma}_{c2}$ with the fast relaxation mechanism suggest that the fast relaxation corresponds to the structure at the high-shear-rate branch and the slower one corresponds to the low-shear-rate branch. Notice that, as the applied shear rate is increased within the shear-banding region, both the slopes of the slow and fast mechanisms increase. We proposed that this is the effect of the disappearance of the lubricating band. Berret and Porte found a similar curve with two main relaxation mechanisms in the time evolution of the negative excess stress after stepping down the shear rate from levels within the shear-banding region to levels below the shear-banding region for wormlike micellar solutions of cetylpyridinium chloride, hexanol, D_2O, and NaCl.[34] These authors attributed this behavior as evidence of the presence of two bands with different structures and claimed that the short characteristic time corresponds to the readjustment of the viscosity of the two coexisting phases to the new shear rate and that the longer characteristic time corresponds to the progressive thinning out and eventual disappearance of the high-viscosity band. However, Berret and Porte did not have data on the mechanical characteristics of the shear-induced aligned phase. By contrast, the relaxation time of the shear-induced band was obtained here, and the similarity with the fast relaxation mechanism in the shear-banding region indicates the presence of this band. Likewise, the similarity of the slow relaxation slope with that of the low-shear-rate branch ($\dot{\gamma} < \dot{\gamma}_{c1}$) demonstrates the existence of this band within the shear-banding region. Unfortunately, we do not have access at present to experimental techniques that allow the observation of the bands. Nevertheless, Makhloufi et al. identified the bands by rheo-optics in a very similar micellar system (cetyltrimethylammonium chloride and NaSal).[16]

Our model is capable of predicting a single relaxation mechanism at very low and very high shear rates (i.e., within the low- and high-shear-rate Newtonian regions). In the shear-banding region, our model predicts two main relaxation mechanisms that qualitatively agree with the experimental data. This is because our model has a small inherent viscoelastic contribution even in the Newtonian regions.

In summary, we have presented oscillatory, steady, and transient data of wormlike micelles that suggest that kinetic-controlled (*fast-breaking*) behavior is a requisite for the appearance of shear-banded flow. A criterion of equal extended Gibbs free energy minima determines the stress plateau and the values of the two critical shear rates.

Acknowledgment. This work was supported by the Consejo Nacional de Ciencia y Tecnología de México (Grants 38681-E and NC-204). E.R.M. recognizes the support of CONACYT, and J.I.E. acknowledges the support of PROMEP (EX-1/2000).

Note Added after ASAP Posting. This article was released ASAP on 7/11/2003 with minor errors in eq 5, captions of Figures 1 and 2, and Table 2. The correct version was posted on 7/14/2003.

LA034052O

(54) Callen, H. B. *Thermodynamics*; Wiley: New York, 1976.
(55) Cates, M. E.; McLeish, T. C. B.; Marrucci, G. *Europhys. Lett.* **1993**, *21*, 451.
(56) Callahan, P. T.; Cates, M. E.; Rofe, C. F.; Smelders, J. B. F. A. *J. Phys. II* **1996**, *6*, 375.
(57) Grand, C.; Arrault, J.; Cates, M. E. *J. Phys. II* **1997**, *6*, 551.
(58) Fischer, P.; Rehage, H.; *Rheol. Acta* **1997**, *36*, 13.
(59) Berret, L. F. *Langmuir* **1997**, *13*, 2227.